A comparative study of oxygen diffusion in PET and PEF using molecular modelling: computational insight into the mechanism for gas transport in bulk polymer systems

Jasmine C. Lightfoot,*,† *Antoine Buchard,*† *Bernardo Castro-Dominguez,*‡ *Stephen C Parker***,†

*jcl68@bath.ac.uk, **chsscp@bath.ac.uk

† Centre for Sustainable and Circular Technologies, Department of Chemistry, University of Bath, Claverton Down, Bath, BA1 7AY

‡ Department of Chemical Engineering, University of Bath, Claverton Down, Bath, BA1 7AY

For Table of Contents use only

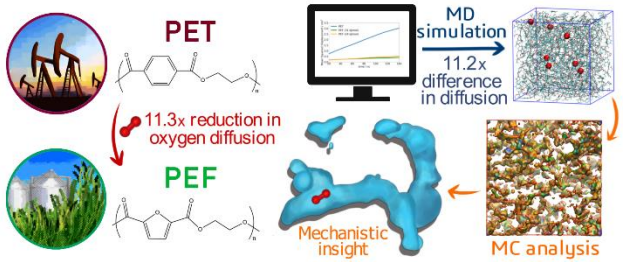

ABSTRACT

Bio-derived polyethylene furanoate (PEF) has recently gained attention as a sustainable alternative to polyethylene terephthalate (PET), amidst environmental concerns over fossil fuel depletion. Herein, we outline a computational approach to investigate the tenfold difference in barrier properties between the two materials, using a statistically robust methodology to predict diffusion coefficients from molecular dynamics simulation. Oxygen diffusion was predicted to a high level of accuracy, at 3.24×10^{-8} $cm^2.s^{-1}$ and 2.88×10^{-9} $cm^2.s^{-1}$ for PET and PEF respectively ($D_{experimental} = 1.16\times10^{-8}$ $cm^2.s^{-1}$ and 1.04×10^{-9} $cm^2.s^{-1}$). Simulations quantifiably demonstrated the contributions of ring flipping chain dynamics on oxygen diffusion, and novel Monte Carlo techniques revealed atomistic insight into the mechanism by which this occurs. Areas of accessible volume within the polymer matrix were seen to converge to facilitate lateral oxygen displacement. Infrequent convergences in PEF, due to subdued polymer chain dynamics and higher system density, accounted for the slower oxygen diffusion relative to PET.

INTRODUCTION

Polyethylene terephthalate (PET) is a semi-crystalline thermoplastic predominantly used for fibers (65%) and packaging (35%) applications.[1–3] The latter includes the production of plastic bottles, containers and films, corresponding to 76%, 11% and 13% of packaging production respectively.[1] The widespread usage of PET in these applications are facilitated by advantageous processability, mechanical and optical properties and high barrier properties towards oxygen and carbon dioxide.[4–6] However, there are increasing environmental concerns over single-use-plastics, particularly for packaging applications - an industry which contributes to 38 % of overall global plastic consumption.[7] Amongst the concerns over fossil fuel depletion, there has been an incentive to replace traditional petrochemically-derived chemicals with those derived from renewable

feedstocks. A proposed sustainable alternative to PET is polyethylene furanoate (PEF).[8] The two plastics are structurally very similar (figure 1); both have an aromatic moiety and an ethylene glycol moiety, joined by linking carbonyl groups. However, in the synthesis of PEF, 2,5-furandicarboxylic acid (FDCA) replaces the use of terephthalic acid, necessary to the manufacture of PET - giving rise to a furan ring in place of a phenyl core. This bifunctional acid can be produced via the oxidation of 5-hydroxymethylfurfural (HMF) - a valuable bio-based precursor which is derived from cellulose.[2,9] A life cycle assessment conducted by Patel and co-workers predicted that complete substitution of PET with biobased PEF, with an annual production of 15 Mt, would reduce greenhouse gas emissions by 45-55 %, and reduce global energy usage by 440-520 PJ per annum.[10]

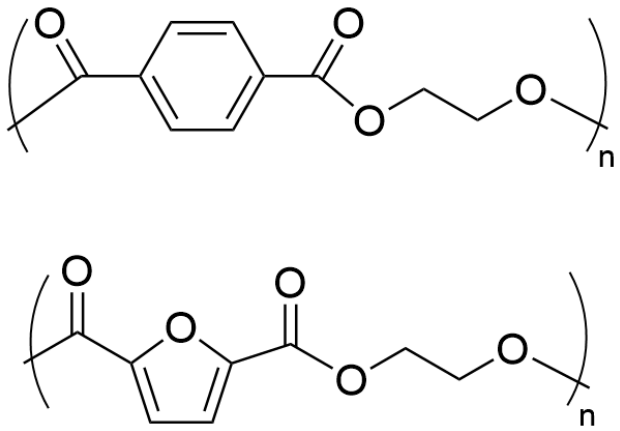

Figure 1. Chemical structures of polymers PET (top) and PEF (bottom).

Practically, PEF may be processed similarly to PET, with the production of plastic bottles by injection stretch blow molding having been demonstrated.[11–13] Its thermal stability is slightly lower than that of PET, with melting and degradation temperatures of 211 °C and 389 °C respectively, compared to 247 °C and 413 °C. Both polymers are semi-crystalline in nature, with glass transition temperatures of 76 °C in PET, and 85 °C in the furan analogue. In comparing the material properties of the two plastics, PEF exhibits a higher modulus than PET, of 3285 MPa vs 2120

MPa.[14] This is attributed to the increased chain rigidity of PEF compared to PET. This same attribute is also considered to be the reason for PEF's tenfold increase in barrier properties over PET, with amorphous samples exhibiting oxygen permeabilities of 0.0107 and 0.114 Barrer respectively at 35 °C.[15,16] This permeability is the product of the gas diffusion coefficient and the solubility of the gas inside the plastic.

Superior barrier properties are essential for a plastic's use as a packaging material, to prevent the transmission of gas contaminants, such as oxygen and water, to the product. This is particularly important in food and beverage packaging, and hence the barrier property requirements for packaging consumable produce are more demanding for increasingly perishable items.[17] The superior barrier properties of PEF over PET are therefore notable; pioneering research conducted by Koros and Burgess[15,18–20] indicate that ring flipping motions are suppressed in PEF, relative to PET. This observation has been confirmed experimentally and attributed to an increased energy for dihedral rotation about the furan moiety through *ab initio* calculations.[21] The suppression of ring-flipping dynamics is thought to account for the increased barrier properties of PEF.[15,22] Sun and coworkers have investigated the effect of the heterocycle dipole moment on the experimentally observed barrier properties of PEF, compared to a sulfur analogue.[23] However, despite the insights that computational simulations could bring to this research, such as through an increased understanding of the transport mechanism, there are currently no computational studies of gas diffusion through PET and PEF, relative to polymer backbone dynamics.

The dynamics of solute gases are characterized in three stages; an initial stage of high mobility, an anomalous diffusion regime and a steady-state regime of Einstein diffusion.[24] For simple liquid systems, diffusion coefficients may easily be calculated from the trajectories of molecular dynamics (MD) simulations, derived from the mean squared displacement (MSD) of the solute in

steady state. However, applying this same method to predict transport coefficients of gasses dissolved in bulk polymer systems under ambient conditions is notoriously difficult.[25] These systems are typically governed by anomalous dynamics and require long simulation times in order to attain Einstein diffusion.[24,26] These have been reported to a respectable accuracy for more permeable polymers, such as PDMS,[27] PE,[28] polypropylene[29] and PIB,[30,31] where solute diffusion is expected in the order of 10^{-5} to 10^{-6} cm^2/s. However, the accuracy of prediction decreases relative to permeability, with solute diffusion in superior barrier plastics ($D \sim 10^{-8}$ - 10^{-9} cm^2/s) often being reported incorrect to 2-3 orders of magnitude.[25,32–34] Moreover, it is common for simulations of this type to analyze solute dynamics over a short timeframes, rarely exceeding several nanoseconds in length. It is likely that the poor accuracy of these studies, limited by the computational resources of the time, are a result of sampling anomalous particle dynamics.[26]

Thus, the challenge for standard MD modelling of oxygen diffusion in PET is the low measured diffusion at 1.16×10^{-8} cm^2/s.[16] Despite its simplicity, predicted oxygen diffusions calculated through MSD exhibited poor agreement with the experimental value, at 1.456×10^{-4} cm^2/s.[32,34] Using transition state theory (TST), a method developed by Gusev and Suter,[25,26,35] Theodorou and coworkers were able to predicted oxygen diffusion in PET at 300 K to a significantly higher level of accuracy (5.4×10^{-8} cm^2/s).[36] However, there are aspects of the TST approach which can limit its application. In the first instance, this method assumes the polymer matrix to be frozen. This leads to difficulties in comparing diffusion in chemically similar polymer systems, as subtle differences in segmental chain dynamics are not taken into account.[36] The method also relies on the implementation of a smearing factor to compensate for elastic thermal motions of polymer atoms.[26] This assumed prior knowledge of the polymer system hinders its application in novel materials. Most notably, however, this method is severely limited by its complexity, with

implementation relying heavily on macros of Accelrys Inc which are no longer publicly available.[37]

Our aim is to characterize and apply a simple and versatile method of predicting the change in diffusion coefficients in polymers. We illustrate our approach by modelling oxygen diffusion through bulk PET and PEF systems using MD simulations. This work-flow (figure 2) makes use of long simulation lengths (200 ns), multiple system samples and duplicates, in order to achieve predicted transport coefficients to the same accuracy as those achieved by TST. To our knowledge, this is the first reported computational study of gas transport in PEF and the first treatment of this polymer using molecular dynamics. By adopting this approach, it is possible to gain a clear atomistic insight into the mechanism for oxygen diffusion and differences in barrier properties between PEF and PET. However, it is critically important that the intermolecular interactions can distinguish selectively the differences in behavior of the chosen polymers, and hence we begin by describing our protocol for testing the chosen force field.

SIMULATION METHODS

A work-flow for assessing the suitability of a given force field in modelling semi-crystalline polymer systems is described in figure 2. This protocol benchmarks published experimental data and *ab initio* density functional theory (DFT) calculations, against which to compare the results of molecular dynamics (MD) simulations. These simulations were specifically designed to check the accuracy of the bonding and non-bonding distance terms and energetics terms of the force field. Further details on simulation methods are outlined below.

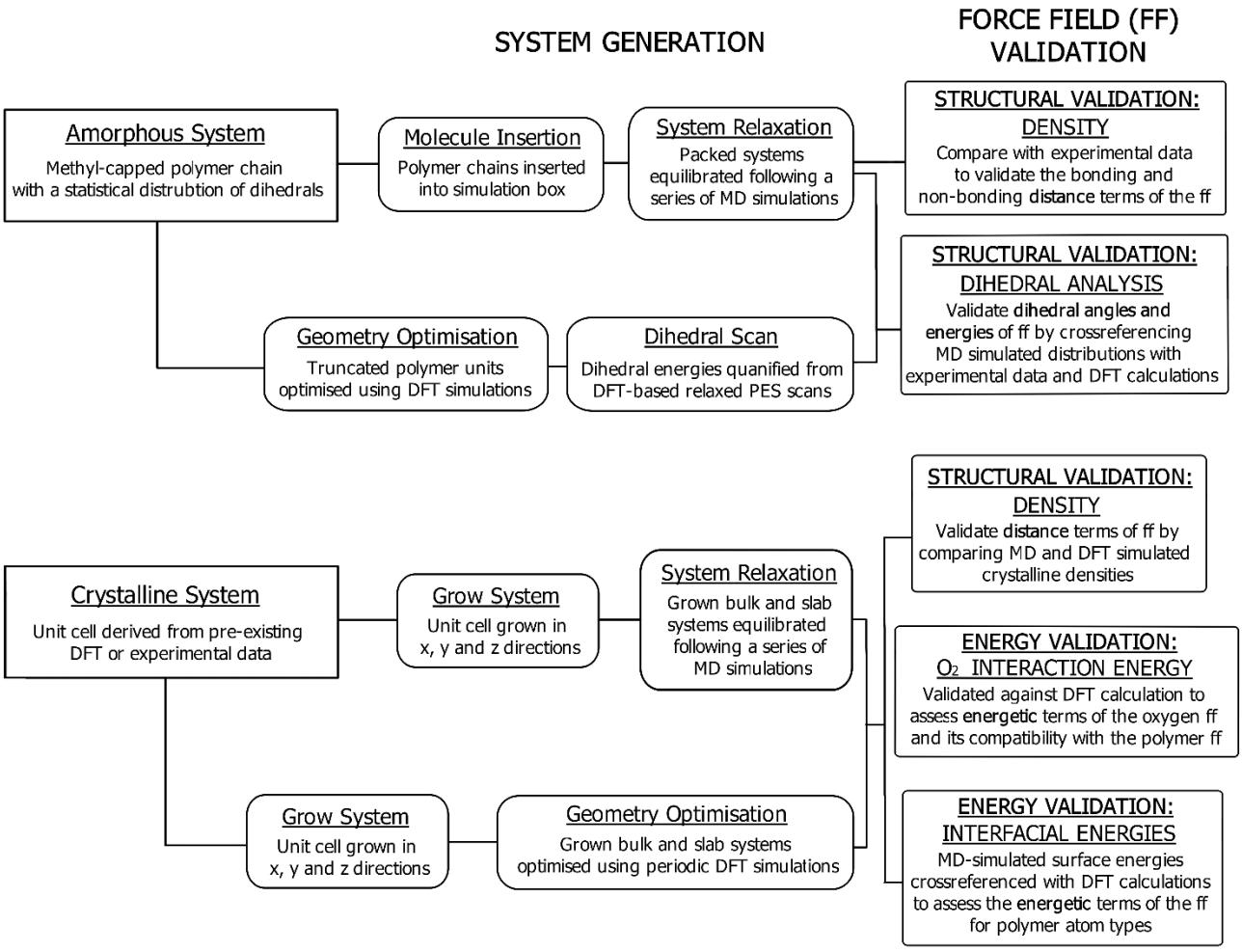

Figure 2: Generalized work flow for validating the force field of semicrystalline polymer systems.

Force Field Validation: Molecular Modelling. The OPLS 2005 force field was employed in molecular dynamics (MD) and grand canonical Monte Carlo (GCMC) simulations. This force field was selected as it was demonstrated reliable representations for π-π interactions, of the sort found in aromatic polyesters PET and PEF.[38] It has also been successfully used in molecular modelling complex carbohydrates and polymers.[39]

Four amorphous systems of both PET and PEF were built, with degrees of polymerization (DP) of 10, 20, 50 and 100. To avoid an over-representation of polar end groups compared to a synthetic

system, where significantly longer chain lengths are attained, simulated polymer chains were capped with methyl groups. OPLS_2005 force field parameters were assigned using DL_FIELD 4.6.[40] Amorphous systems were prepared by following a series of equilibration MD simulations, employing an NPT ensemble; systems were initially held at 750 K and 100 atm for 2 ns, followed by a gradual decrease over 1 ns to ambient conditions. Systems were then exposed to 4 cycles of annealing over a 10 ns NPT simulation, following a temperature gradient from 298 K to 1200 K to 298 K. A final 1 ns NPT simulation at ambient conditions allowed for changes to box dimensions following annealing. All equilibration simulations employed a Berendsen thermostat and barostat. Production simulations used a Nose-Hoover thermostat and, when relevant, MTTK barostat.

Atomistic oxygen models developed by Monticelli[41] were used for this research. The validity of the polymeric force fields and those of atomistic oxygen, particularly the cross terms, were assessed by comparing the energetic data with that calculated from van der Waals corrected DFT, and through comparisons with pre-existing experimental data. Of the latter, density was critical – as incorrect portrayal of this property could impact the movement of the penetrant throughout the polymeric matrix.

Crystalline systems of PEF and PET were built from their respective unit cell structures - derived from X-ray fiber diffraction[42] and DFT[43] respectively. These were grown using METADISE,[44] to generate packed bulk and slab crystalline systems (figure 3). Slab surfaces were generated such that the aromatic entity lay flat at the polymer vacuum interface; formed along the (0 1 0) Miller index for PEF and the (1 0 0) Miller index in the case of PET. These systems were modelled, using the DL_POLY 4 package[45] to carry out MD simulations. Equilibration in the NσT ensemble allowed for anisotropic changes to box dimensions, lasting 1 ns. A surface scan was conducted, to identify the most favorable sites for interaction. Herein, oxygen was placed above PEF and PET

slab surfaces, following a 5 Å grid at a distance of 2 Å from the surface. Short MD simulations of 50 ps were performed at each position, with oxygen frozen in place. Sites of the lowest energy interaction, as determined by these preliminary scans, were then further equilibrated for 1 ns. Simulations were run at room temperature and at 1 K - the latter was used to compare energetic data with that calculated from DFT.

Force Field Validation: Density Functional Theory (DFT). DFT was used to complement this research and provide further validation to the parameters selected for MD simulations. Discrete *ab initio* calculations were performed when considering individual bond energies, whereas periodic DFT, employing periodic boundary conditions, was used when considering an extended bulk structure.

The former was computed using the Gaussian 16 software,[46] at the B3LYP level of theory with the 6-311++G(*d,p*) basis set. Truncated, single repeat units of PEF and PET were considered for these calculations; initial conformational searches and geometry optimizations allowed for the identification of the most stable conformer. Dihedral rotations were analyzed using a Relaxed Potential Energy Surface (PES) Scan, at 5° increments, to allow for calculation of dihedral bond energies.

Crystalline bulk and slab systems of PET and PEF were simulated using Density functional theory (DFT) calculations through the Vienna Ab-initio Simulation Package (VASP) code[47–49] These were performed using the PBE functional, within which projector augmented wave pseudopotentials and a plane wave cutoff of 500 eV were used, with the sampling of the Brillouin zone sampled using a Monkhorst-Pack grid for the bulk and slab materials. Relaxation of the structure considered to have converged when the forces acting on all atoms are below 0.01 eV/atom, and the electronic energies converged to 1×10^{-6} eV/atom. As with our earlier studies[50]

we used the optB86b-vdW van der Waals corrections to better describe the interactions, particularly between O_2 and the polymers.[51]

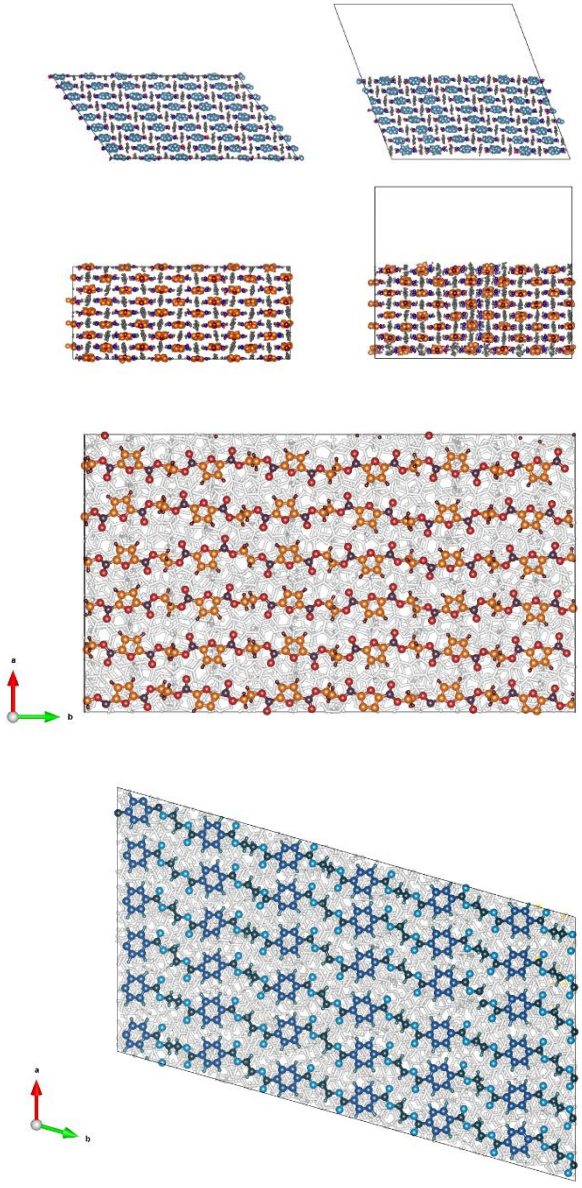

Figure 3. Bulk and slab systems of crystalline PET (blue) and PEF (orange), generated along the (1 0 0) and (0 1 0) Miller indices respectively such that aromatic moieties lay planar along the polymer-vacuum interface.

Diffusion Modelling: Grand Canonical Monte Carlo (GCMC). Grand canonical Monte Carlo using the DL_MONTE code[52] was used to saturate amorphous PEF and PET systems with oxygen. Due to the dynamic nature of the polymeric systems, MD and GCMC were run in tandem, wherein configurations were sampled with Monte Carlo every 10ps of a 0.5 ns NVT MD simulation. Oxygen insertion, displacement and rotation moves were performed over 1 000 000 MC steps, with a weighting of 60%, 20% and 20% respectively. The most saturated configuration of the 50 tandem MC simulations was selected for subsequent MD diffusion simulations of PEF. To allow for a direct comparison, PET configurations were selected to match the concentration of the PEF system at an equivalent chain length. The SCAN function of DL_MONTE was employed to probe the energy profile of a system, at each point along a 0.5 Å grid. This allowed for the identification of potential sites for oxygen occupancy and hence regions of 'accessible volume'.

Diffusion Modelling: Molecular Dynamics (MD). In modelling diffusion, MD simulations were performed using the GROMACS package,[53–55] due to its increased efficiency in simulating the pre-equilibrated amorphous polymer systems over longer MD timescales. Once the polymer systems were saturated with oxygen, they were relaxed via a 1 ns 298 K MD simulation, using the NPT ensemble to allow for volume changes to accommodate the additional oxygen molecules. Subsequent NVT simulations, using random seeding to generate initial velocities, were used to analyze oxygen diffusion. Unless otherwise stated, oxygen MSD was averaged across 5 duplicate simulations for each of the four variants of the polymer system. Oxygen diffusion coefficients were calculated from the linear region of the average MSD curve for each polymer type, discounting an initial region of anomalous diffusion, associated with system equilibration, and the final portion of the simulation, where poor statistics led to spurious results in MSD calculation. A trendline of the form $y = mt + c$ was fitted to this region, where the linear relationship between

MSD and time was indicative the Einstein diffusion regime having been attained. From this linear regression, a diffusion coefficient was calculated following the Einstein relation:

$$(1) \qquad \mathrm{D} = \frac{1}{6\mathrm{N}} lim \frac{\delta}{\delta t} \sum_{t=1}^{\mathrm{N}} \langle |\mathbf{r}_i(t) - \mathbf{r}_i(0)|^2 \rangle$$

Wherein D is the diffusion coefficient, $\mathbf{r}_i$ is the position vector of the particle *i* and $\langle |\mathbf{r}_i(t) - \mathbf{r}_i(0)|^2 \rangle$ the average MSD of all oxygen molecules.

RESULTS

Results of this study are presented in three sections; force field validation, diffusion modelling and finally atomistic insight into the diffusion mechanism. In the former, we demonstrate that the molecular models generated for PEF and PET are reliable and accurate representations of real systems. In diffusion modelling, we propose a method for predicting diffusion coefficients of oxygen through these polymeric systems. In demonstrating successful prediction of diffusion behavior in the previous section, we conclude with an atomistic scale investigation into the diffusion mechanism; probing the extent to which ring-flipping dihedral rotations affect oxygen diffusion coefficients between PET and PEF. Herein we also perform a detailed analysis of the hopping behavior of oxygen, ultimately responsible for lateral diffusion throughout the polymer system.

Force Field Validation: Crystalline Systems. An initial study was conducted, to validate the use of the OPLS_2005 force field in modelling polymeric PET and PEF systems. Crystalline systems of both polymers were generated and simulated using both DFT and MD techniques. In the first instance, density measurements allowed for a comparison between systems treated with DFT, MD and experimental values; these results are presented in table 1.

Table 1. Experimental and simulated densities of crystalline PET and PEF systems

	$\rho_{MD,298K}$ / g.cm^{-3}	$\rho_{MD,1K}$ / g.cm^{-3}	ρ_{DFT} / g.cm^{-3}	$\rho_{experimental}$ / g.cm^{-3}
PET	1.503	1.574	1.638	1.559 [a]
PEF	1.547	1.636	1.678	1.562 [b]

Crystalline densities predicted by this study are compared with experimental results taken from [a]Liu and Geil[56] and [b]Mao, Kriegel and Bucknall[42]; herein unit cell dimensions have been derived from X-ray diffraction data.

The systems simulated with MD were able to replicate experimental densities well, with the PET crystalline system exhibiting the highest discrepancy, at 3.6% error. The error associated with the PEF crystalline system, relative to the experimental density of crystalline domains in this polymer, was less than 1%. Systems were also simulated in MD at 1 K, to compare the densities predicted using an all-atom force field with those predicted from *ab initio* quantum calculations. Systems simulated in DFT were more compact due to the extent of atomic movement between ionic relaxation steps, which is more limited in DFT than what can be achieved over the course of a 1 ns MD simulation. However, the predicted densities compared favorably between simulation methods, with values within 2.5-3.9% of each other. Agreement between experimental observations, DFT calculations and the results of MD simulations indicated that the bonding and non-bonding distances included in the OPLS_2005 force field parameters were appropriate representations for these systems.

Employing DFT calculations as a benchmark to compare the results of MD simulations is common in force field validation and development.[57–59] One such parameter which is useful in assessing energetic terms is interfacial surface energy; defined as the excess energy of a surface exposed to vacuum, per unit area. In this context, this cleavage energy can be used to quantify the energy of interaction between stacked polymer chains. Thus, the suitability of the OPLS_2005

force field in modelling PET and PEF was further assessed by comparing the interfacial energy of crystalline polymer systems, calculated from equation 2,[60,61] between DFT and MD simulations.

$$E_{surface\ energy} = \frac{\frac{1}{2}(E_{slab} - E_{bulk})}{A_{slab}} \quad (2)$$

Table 2. Interfacial surface energies of crystalline PEF and PET systems, calculated from MD and DFT simulations

	$E_{surface,DFT}$ / J.m^{-2}	$E_{surface,MD}$ / J.m^{-2}
PET	0.150	0.166
PEF	0.157	0.176

The surface energies of both polymer systems calculated through MD were very similar to those calculated through more accurate quantum methods (table 2). In general, we find that DFT surface energies are lower than those from force fields, because of the explicit treatment of the electronic polarizability.[62] Both simulation methods indicated that a higher energy was required to separate PEF layers than PET - which, although not directly comparable, is intuitively in agreement with the material's higher density and its higher tensile modulus and strength.[14] The good agreement between MD and DFT simulations indicated that the energetic parameters of the OPLS_2005 force field were suitable for modelling PEF and PET.

As simulated oxygen diffusion is dependent on force field parameters of atomistic oxygen, it was also necessary to validate the chosen oxygen model, with particular emphasis on its suitability in a mixed polymer/ oxygen system. This was performed by calculating the interaction energy of oxygen on a polymer slab surface with both MD and DFT simulations. Using *ab initio* calculations as a benchmark, contrasting the two results, presented in table 3, allowed for further validation of

force field accuracy. Interaction energy was calculated from equation 3,[57] employing the Monticelli[41] model to define atomistic oxygen.

$$(3) \qquad \mathrm{E}_{interaction} = E_{slab+\mathrm{O}_2} - \mathrm{E}_{slab} - \mathrm{E}_{\mathrm{O}_2}$$

Table 3. Interaction energy of oxygen with polymer surface, as calculated with MD and DFT

	$\mathrm{E}_{interaction,MD}$ / kJ.mol^{-1}	$\mathrm{E}_{interaction,DFT}$ / kJ.mol^{-1}
PET	-10.9	-10.2
PEF	-13.8	-13.0

Energies were individually tested with oxygen located at each point across a 5 Å grid. In both PET and PEF, oxygen exhibited a favorable interaction energy with the polymer surface at all locations across the grid. It was possible to visualize this attractive force by allowing oxygen to move freely inside the vacuum. Oxygen coordinates at each timestep of the multiple simulations were extracted and plotted in the form of a heatmap, in relation to the polymer-vacuum interface with kernel density estimation algorithm (figure 4). The higher density of oxygen in proximity to the polymer slab demonstrates the energetic preference of oxygen to adhere to the slab surface. Furthermore, by probing the density rather than interaction energy, we gain information on relative free energies of adsorption. In both PET and PEF, there was no particular position at which interaction was any favorable - which can be expected due to the regularity and homogeneous nature of these surfaces.

The energy of oxygen interaction, as obtained through DFT and MD, were very similar for both PET and PEF systems. The excellent agreement between these two values demonstrated the suitability of the Monticelli oxygen model for future MD and GCMC simulations. This agreement

also indicated good compatibility between this oxygen model and force field parameters assigned to the polymers.

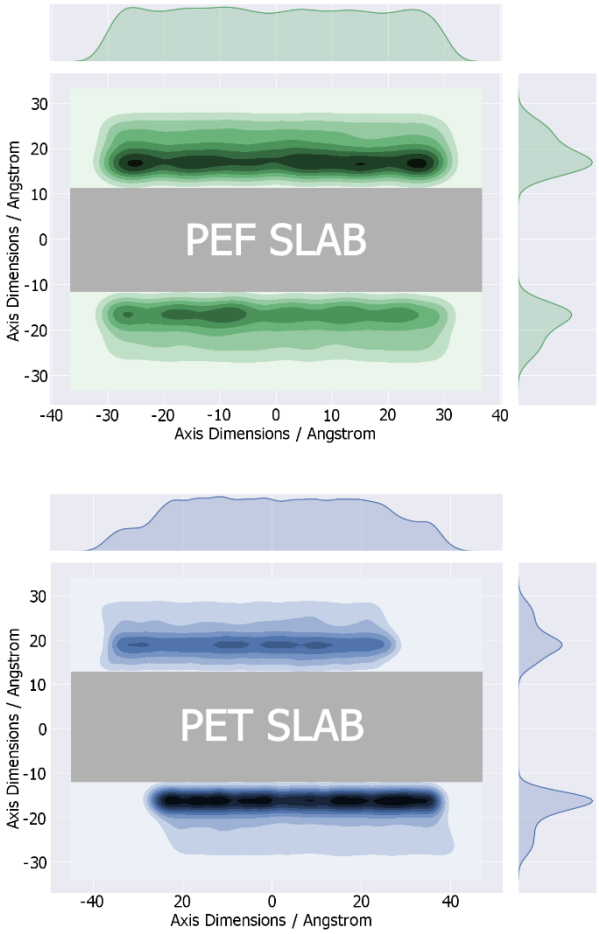

Figure 4. A heatmap of atomistic oxygen coordinates throughout MD simulations, demonstrating the energetic preference for molecules to adhere to PET and PEF surfaces.

Amorphous systems. Four amorphous systems of PET and PEF were considered in this study, with DPs of 10, 20, 50 and 100. A comparable total number of atoms was maintained between systems of either polymer, by reducing the number of chains present. These systems were equilibrated following the previously outlined annealing procedure, to allow the chains to pack and relax to their lowest energy conformations. Tables 4 and 5 detail the number of chains and

atoms contained in each PEF and PET system respectively, in addition to their corresponding densities.

Table 4. Density of amorphous PEF systems of increasing degrees of polymerization

DP_{PEF}	Number of chains	Number of atoms	Density / $g.cm^{-3}$
10	36	7164	1.390
20	18	7002	1.390
50	8	7672	1.390
100	4	7636	1.410

Table 5. Density of amorphous PET systems of increasing degrees of polymerization

DP_{PET}	Number of chains	Number of atoms	Density / $g.cm^{-3}$
10	36	8244	1.265
20	18	8082	1.269
50	8	8872	1.268
100	4	8836	1.269

Each polymer system, regardless of its degree of polymerization, converged to approximately the same density following the previously outlined equilibration procedure. In the case of PEF, the densities attained very closely matched the experimental value of a wholly amorphous sample, of 1.435 $g.cm^{-3}$.[63] A higher discrepancy was observed for equilibrated PET systems. However, the densities achieved across all four systems were consistent, and all came within 5.3 % error of the amorphous experimental density of 1.335 $g.cm^{-3}$.[63]

As recent work suggests that the diffusion of penetrants through PET and PEF is heavily influenced by ring flipping chain dynamics,[15,18–20] it is therefore important to ensure that the force field models were able to replicate the chain conformations and torsions of their experimental counterparts. Thus, we performed an in-depth analysis on key dihedral angles to ensure sensible and realistic polymer conformations were attained, with accurate energy barriers for dihedral rotation about the carbonyl/aromatic moiety. This was quantified by performing a series of DFT calculations on truncated PEF and PET structures. The bonds of interest, highlighted in figure 5, were the O=C−C−O and O=C−C−C dihedrals for PEF and PET respectively. The three possible orientations of a PEF unit are depicted in figure 7. *Anti-anti*: the two adjacent carbonyl C=O bonds are both 180° to the C−O furan bond. *Syn-syn*: both carbonyl C=O bonds are at 0° in line with furan C−O bonds. *Syn-anti* or *anti-syn*: a combination of the two. Due to the horizontal symmetry plane running through the phenyl substituent in PET, *anti-anti* and *syn-syn* conformations are equivalent - resulting in only two distinct orientations.

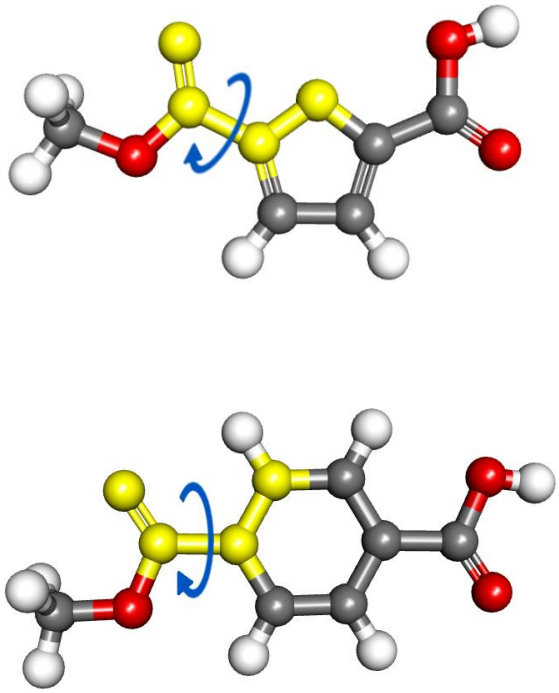

Figure 5. Truncated PEF (top) and PET (bottom) structures, with dihedrals highlighted in yellow subject to a 360° relaxed potential energy surface scan

The energy barrier for rotation was calculated with DFT, through a 360° potential energy surface (PES) scan about the highlighted dihedral bond. In agreement with previous research,[21] this was found to be higher in PEF than in PET - at 30.9 kJ.mol^{-1} and 24.4 kJ.mol^{-1} respectively. To ensure that the subtle differences between the dihedral energies of these PET and PEF bonds were replicated in MD, an analogous scan was performed. The energetic dihedral bonding terms of the carbonyl/furan 4-body interaction were adjusted, to increase the energy barrier for dihedral rotation in PEF from 25.1 kJ.mol^{-1}, as measured from the original OPLS_2005 terms in MD simulation, to 31.0 kJ.mol^{-1} (see supporting information). The rotational energy for PET exhibited good agreement with DFT calculation, measured as 24.2 kJ.mol^{-1} using unmodified force field parameters.

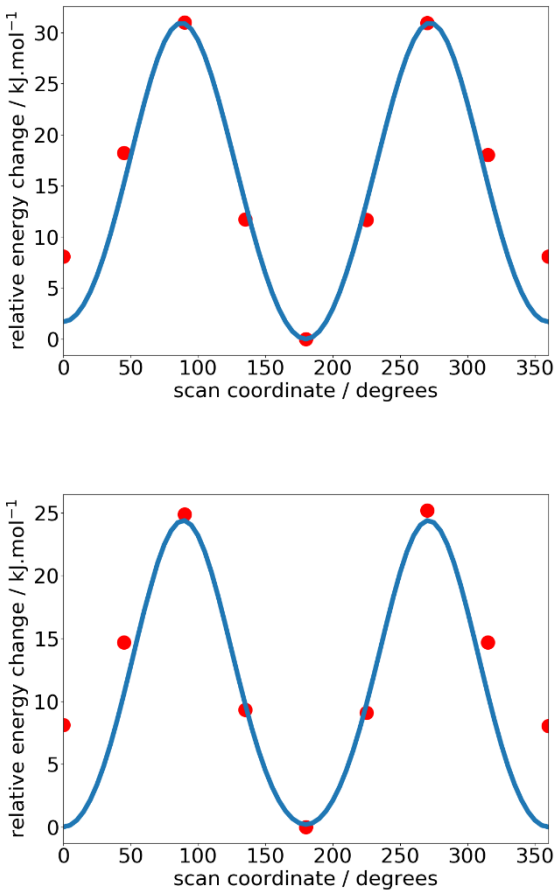

Figure 6. A 360° potential energy surface scan around the O=C−C−O dihedral in PEF (top) and the O=C−C−C bond in PET (bottom). The blue curve represents relative energies obtained from DFT and overlayed red points from equivalent force field/ MD simulations.

These results allowed for conformations to be ranked in order of increasing energy, as depicted in figure 7. In PEF, the *anti-anti* conformation was most stable. Eclipsing of the C=O / C−O bonds was associated with an energy penalty of +1.7 kJ.mol^{-1} per repeat unit, resulting in *anti-syn* and *syn-anti* conformations being less stable. The *syn-syn* conformation was found to be the highest in energy, with both C=O bonds eclipsing C−O furan bonds. This hierarchy matches that reported by Sousa and co-workers, who used DFT calculations to demonstrate an energetic preference for *anti*

conformations.[21] These trends were correctly assimilated in MD by the OPLS force field, as demonstrated through the distribution of select dihedrals across 200 ns simulations (figure 8). O=C−C−O bonds exhibited preference towards the *anti* conformation, with 180° being the most populated angle over the course of the simulation. In PET, the analogous dihedral angles of O=C−C−C at 0° and 180° are equivalent and were therefore equally populated. In both PEF and PET systems, the ethylene glycol O−C−C−O favored a gauche orientation, at 60° and 300°. This is in agreement with Sousa's computational findings of gauche being the lowest energy conformation for this dihedral.[21]

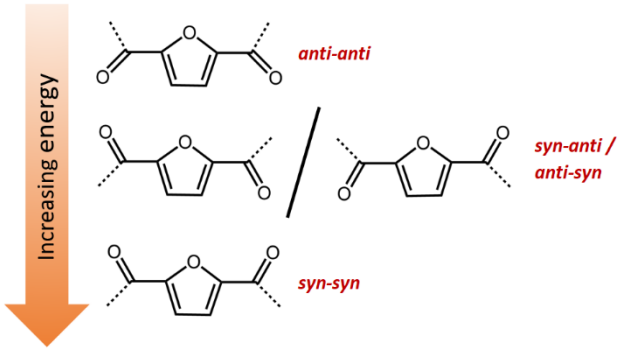

Figure 7. PEF conformations in order of increasing energy, as determined from DFT calculations.

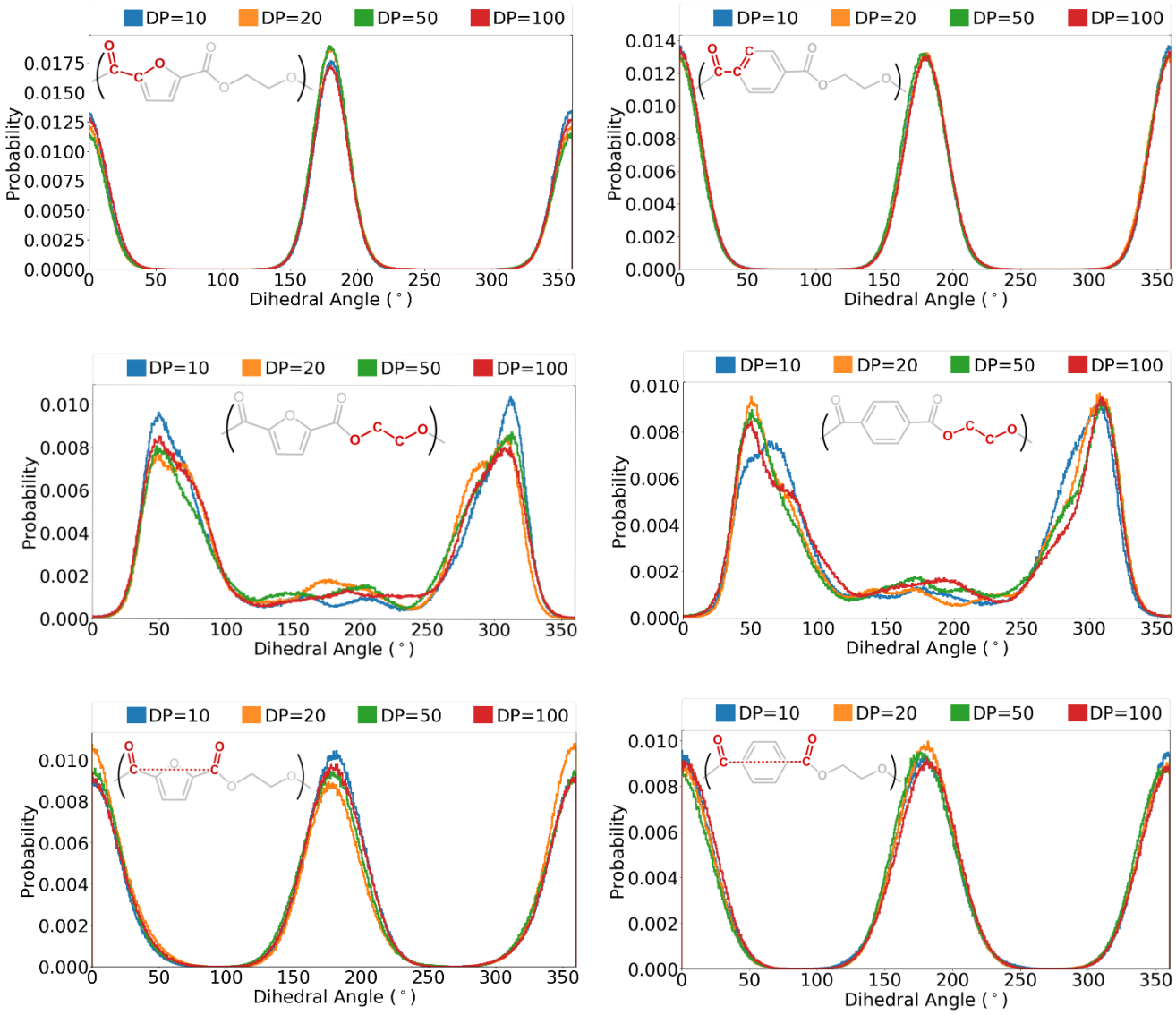

Figure 8. Distributions of key dihedral angles in PEF (left) and PET (right), gathered over the course of a 200 ns MD simulation.

Sousa *et al.* also performed an experimental investigation on crystalline and amorphous PEF samples. In agreement with our models, infrared spectra also indicated that the *gauche* conformation was dominant for ethylene glycol moieties in amorphous PEF. The same observation has been noted for amorphous PET samples, with a distinctive peak at 1340 cm^{-1} that is often used to infer the degree of crystallinity of polymers (relative to the *trans* peak at 1370 cm^{-1}, indicative

of crystalline domains). Further reflected in our PEF models, Sousa and coworkers noted that the *anti* conformation of O=C−C−O furan bonds was dominant experimentally, but that a considerable percentage of *syn* conformers prevailed among disordered chains.[21] The distributions of these dihedrals closely followed the same trends in all four system sizes of both PEF and PET (figure 8). This indicated that chain conformations were analogous in all relaxed systems of a given polymer type.

Throughout structure generation and analysis, we have demonstrated that these crystalline and amorphous PEF and PET models are accurate and are an appropriate representation of their real systems. Through comparison with quantum calculations and experimental results, we have thoroughly assessed and validated the force field in representing both polymers. Structural validation was achieved via density checks and dihedral distribution analysis and energetic validation from calculations of interfacial surface energy and oxygen interaction energy. Having developed and substantiated PEF and PET models, we now proceed to investigate diffusion behaviors upon saturating these systems with oxygen.

Modelling Diffusion. It is understood that the pathway for diffusion of gasses dissolved in polymers proceeds via amorphous domains. The presence of impenetrable crystal fractions act as a barrier for the diffusing particle, causing it to take a more tortuous pathway and hence lower the transport coefficient.[6,64,65] To ensure that the lack of oxygen solubility in the crystalline domains was replicated, we probed this using Grand Canonical Monte Carlo and MD simulations. Indeed, even at very high oxygen partial pressures - exceeding 1000 atm - crystalline systems of PEF and PET were found to be totally impermeable to oxygen insertions, equating to an effective oxygen solubility of zero within the polymer. The diffusion pathway through these modelled crystalline

regions was further investigated with MD simulation, by considering interfaces of crystalline polymer slabs, described above, in contact with highly pressured layers of atomistic oxygen. We found no oxygen penetrated the crystalline surfaces, which gives further evidence that oxygen diffusion in these semicrystalline polymers cannot proceed through crystalline domains. Thus, we focused on oxygen diffusion through amorphous PET and PEF models for the comparison with experimental diffusion data; where the starting positions for oxygen molecules were obtained using GCMC to ensure chemically sensible locations within the systems.

The low oxygen solubility and slow diffusion in these systems present a challenge when modelling transport coefficients through molecular dynamics, as the concentration of mobile species in a barrier material is intrinsically low. It is therefore necessary to ensure that sufficient data is collected for the calculated oxygen diffusion coefficient to be representative of an average system. Poor statistics and the resultant high variation between calculations can be overcome by gathering data from several duplicate simulations. This is demonstrated in Figure 9, where the oxygen MSD over 200 ns simulations is averaged over an increasing number of duplicate simulations of a PEF (DP=10) system.

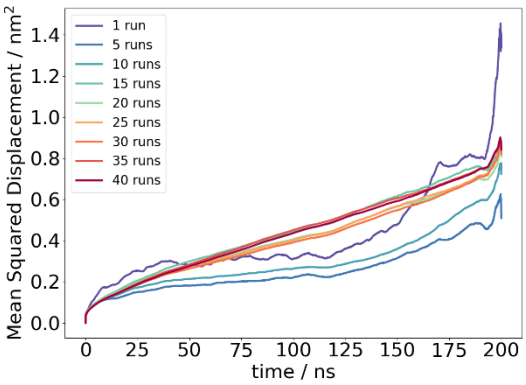

Figure 9. A plot of oxygen MSD against time in PEF (DP=10), when averaged over an increasingly large dataset.

The increasing linearity of this series when sampling over an increasingly large dataset demonstrates the inadequacy in calculating oxygen diffusion in PEF from a single simulation. This is due to the high variation in oxygen displacement between repeats of the same system, emphasized by the inherently sporadic diffusion mechanism, wherein oxygen jumps through temporary channels between entangled polymer chains. The observed high variation in diffusion coefficients between duplicate runs can therefore be explained, because lateral oxygen movement ranges from zero - whilst the oxygen is locked into position by surrounding bulk polymer - to high - when polymer dynamics allow for the molecule to experience a jump. The magnitude of displacement therefore varies significantly with the frequency of oxygen escaping its occupied position.

The variation in diffusivity is illustrated by considering the distribution of the maximum displacement achieved by each oxygen atom across the 40 duplicate 200 ns simulations in PEF (figure 10). Whilst many oxygen molecules are trapped in their initial positions throughout the simulation, the most mobile of molecules are displaced almost a full cell-length from their original site. Therefore, although the average maximum MSD experienced by oxygen in PEF is low due to the number of immobile species, the displacement arising from a jump event is still significant. This can further be demonstrated by visualizing the collective oxygen trajectories of these simulations, where a considerable portion of the simulation cell is explored (see supporting information). The significant variation in the molecular transport, influenced by the local polymeric environment which surrounds it, reinforces the need to a treat a statistical distribution

of penetrant molecules over a number of duplicate simulation cells as a collective, rather than to consider the MSD of each oxygen molecule individually.

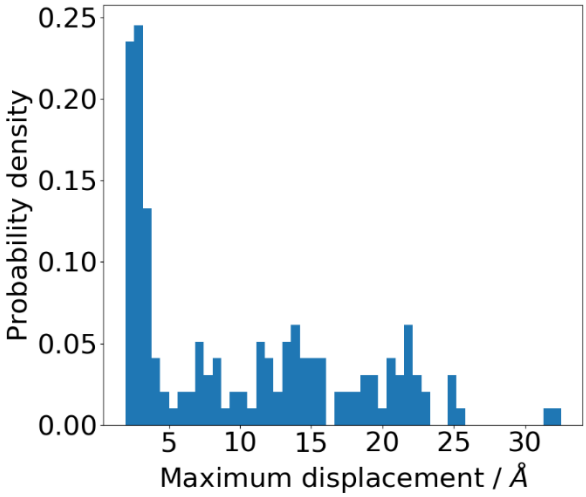

Figure 10. A histogram showing the maximum RMSD attained by each oxygen across 40 200ns simulations, in PEF (DP=10).

As seen in figure 9, no significant changes were observed to the gradient of the average MSD curve upwards of 15 duplicate simulations, despite the additional computational resources required. This highlights limitations and sources of error in previous diffusion modelling studies, wherein coefficients have been derived from the MSD of a single simulation. Going forward, diffusion coefficients of oxygen in PEF and PET systems were therefore calculated over 20 individual 200 ns simulations. This was divided between the four uniquely generated systems, to have a representation of polymers at a range of chain length, and to minimize size effects and those arising from potential deviations between systems.

Due to the anomalous mechanics governing the initial stages of the simulation, all MSD curves initially exhibited a region of high mobility, before entering a linear regime associated with Einstein diffusion. Oxygen diffusion was therefore calculated from the linear region, discounting the initial region of anomalous diffusion and final portion of the curve, where decreased statics

lead to erratic and spurious results. On average, for a 200 ns simulation, diffusion was therefore sampled over 126 ns, with $R^2 > 0.99$ fitting the linear regression in each case. To ensure that the latter stages of the simulation were indeed governed by the Einstein diffusion regime and that the sampled data was representative of an average polymer system, the acquired MSD curve of oxygen in PEF was compared to that calculated across 40 duplicate 600 ns simulations (figure 11). By applying the Einstein relation to the linear region of both curves, diffusion coefficients were calculated within just 1.5×10^{-11} $cm^2.s^{-1}$ of one another, in spite of the 6 times increased computational cost and resources required to run the latter. This demonstrated that the initial study of 200 ns allowed for sufficient time to attain a steady state, governed by Einstein diffusion mechanics. This was further evidenced when considering the logarithmic plots of log(MSD) against log(time), where a linear 1:1 proportionality between the two variables is indicative of Einstein diffusion. This relationship was attained for all polymer systems during the time period in which diffusion coefficients were calculated, following the linear equation log(MSD) = log(time) + log(6D) (individual logarithmic graphs for each polymer system are provided in the supporting information). The quoted values for oxygen diffusion in PET and PEF (table 6) were subsequently normalized against the effective diffusion of polymer chains, to take negate any drifting of the whole system in space.

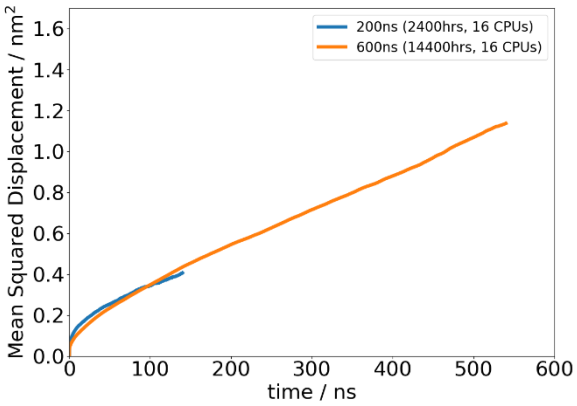

Figure 11. A plot showing the average MSD of oxygen collected over 20 duplicate 200 ns simulations, and 40 duplicate 600 ns simulations.

Table 6. The average predicted diffusion coefficient of oxygen in bulk PEF and PET systems at 298 K, with respect to the experimental values.

	$D_{simulated}$ / $cm^2.s^{-1}$	$D_{experimental}$ / $cm^2.s^{-1}$
PEF	$2.88 \pm 0.62 \times 10^{-9}$ [a]	1.04×10^{-9} [b]
PET	$3.24 \pm 0.51 \times 10^{-8}$ [a]	1.16×10^{-8} [b]

[a] This study. [b] Koros *et al.*[15]; amorphous films prepared from a melt press procedure, diffusion measured at 35°C using a transient timelag experiment at 1 atm O_2.

Overall, the diffusion coefficient predictions from MD simulations showed very good agreement with the experimental values. It is possible that the slight overestimation of transport coefficients in these models is due to their fully amorphous nature; as even small domains of crystallinity exhibited by the synthetic polymer will result in decreased oxygen diffusion.[6,64,65] Diffusion in PEF was calculated as 11.3 times slower than in PET, compared to the experimentally determined

11.2 times difference. Not only does this method provide realistic comparative results between both plastics, but the absolute values of predicted oxygen diffusion coefficient are also very similar to their synthetic counterparts.

These simulated coefficients are considerably more accurate than previously reported attempts to predict oxygen diffusion in PET through MSD,[32,34] which have been incorrect by up to three orders of magnitude. This improvement is likely due to the increased simulation length and statistical improvement owing to the number of duplicate systems analyzed using this method.

Diffusion Mechanism. The conclusions of a series of pioneering experimental studies conducted by Koros *et al.*,[15] indicated that the tenfold reduction in oxygen diffusion between PEF and PET were related to inherent differences in the molecular structure, and specifically the ring rotation motional processes between the two plastics. The noteworthy and thorough investigation employed detailed ^{13}C NMR spectroscopy to observe the suppression in furan ring-flipping relative to phenyl ring-flipping in PET samples. From this, the group stipulated that the reduction in diffusion between the two plastics was caused by a hindrance in furan-ring flipping in PEF. These experimental observations are in-line with our electronic structure calculations, which give the energy barrier for rotation of dihedral ring-flipping motions (see figure 6) as approximately a third higher in furan than phenyl moieties (31.0 kJ/mol^{-1} *cf.* 24.4 kJ.mol^{-1}).

In order to analyze the difference in ring-flipping motions between PEF and PET models, and importantly the effect of this on oxygen diffusion, the number of ring flips were quantified over the course of a 200 ns MD simulation. A ring flip was said to have occurred with a change in dihedral of over 120° between timesteps. In addition to the PEF and PET systems, with rotational barriers matching that calculated from DFT, a hypothetical PEF system was also simulated - with the same starting configuration, but with an energy barrier for ring flipping set to match the PET

system (~24 kJ.mol^{-1}). The number of flips per residue increased to that of PET, and impacted the associated oxygen diffusion coefficient, as listed in table 7.

Table 7. Simulated oxygen diffusion coefficient and frequency of ring flipping motions in PEF and PET systems.

	PEF (31 kJ/mol)	PEF (24 kJ/mol)	PET (24 kJ/mol)
number of ring flips / repeat unit	0.4 ± 0.1	1.6 ± 0.4	1.4 ± 0.1
$D_{simulated}$ / cm^2.s^{-1}	2.88 ± 0.62 ×10^{-9}	4.99 ± 1.06 ×10^{-9}	3.24 ± 0.51 ×10^{-8}

These results support the assertion made by Koros *et al*.[15], that the reduced chain dynamics of PEF results in a lowering of oxygen diffusivity throughout the polymer matrix. It is clear from these simulations that a strong correlation exists between increased ring flipping activity and an increase in gas diffusivity in the bulk polymeric matrices. Indeed, the frequency of ring flipping appears to be dictated by the energy barrier for dihedral rotation, as the number of these occurrences does not differ significantly between PET and PEF systems when rotational energy barriers are the same. However, the number of ring flips experienced by PEF residues decreases by a factor of 3.75 upon increasing the energy barrier for rotation in PEF to a more realistic value of 31.0 kJ/mol^{-1}. This results in a decrease to the oxygen diffusion coefficient by a factor of 1.7. These findings were consolidated with the results from a larger data set, to ensure the correct identification of any differences in oxygen diffusion between the two subtly different PEF systems, and reaffirm the conclusions herein drawn. Calculation from a set of 55 duplicate simulations of each PEF system led to a 1.4 times reduction in oxygen diffusion. The results support the view

that stiffer chain dynamics and rotation, first highlighted by Koros and Burgess, result in lower diffusion and suggest that a further increase in chain stiffness would lower diffusion still further.

However, whist the difference in dihedral rotation between PEF and PET undoubtably contributes to the experimentally observed tenfold difference in oxygen diffusion between PET and PEF, these simulations suggest oxygen diffusion is also impacted by other factors. With equal energy barriers and occurrences of ring flipping, there remains 6.5 times difference in simulated diffusion between PEF and PET. This is likely due to the higher system density in PEF, and energetic interactions between polymer and penetrant. Indeed, the MD simulated interaction between oxygen and polymer slab surfaces is 3 $kJ.mol^{-1}$ more favorable for PEF than in PET. This stronger adhesion to PEF chains could result in increased retention and therefore slow the traversing of oxygen molecules across the polymer system.

The importance of system density on diffusion becomes apparent when considering the oxygen diffusion mechanism. Oxygen occupies regions of empty space between entangled polymer chains. Analyzing the root mean squared displacement (RMSD) of oxygen over the course of a simulation reveals that this region of accessible space acts as a cage for oxygen. Although the penetrant molecule can be seen to rattle within this cage, with sporadic displacements of 2 Å in magnitude, significant traverse diffusion from its initial location is inhibited. This explains the low diffusion coefficients of penetrants through bulk polymeric matrices. Translational diffusion can only occur when small movements in the polymer conformation result in temporary channels connecting adjacent regions of accessible space. If this occurs to an occupied cage, with oxygen moving in the correct direction with a sufficient velocity, the penetrate molecule is able to jump to an adjacent site (see figure 12).[24,25,66]

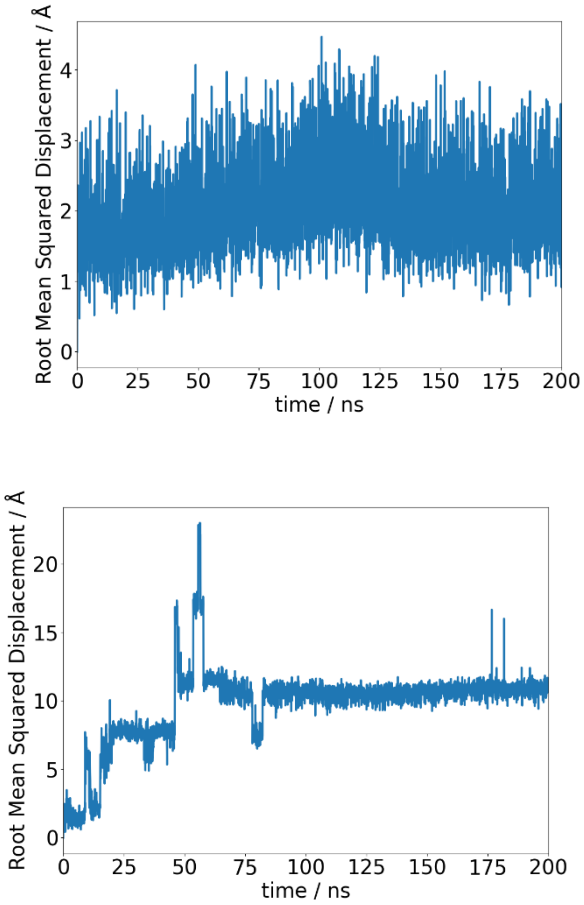

Figure 12. RMSD plots of two oxygen penetrants in an amorphous PEF system; top exhibits rattling behavior with hindered lateral diffusion, and bottom demonstrates significant movement from its original position

In this study, the mechanism for this hopping behavior has been analyzed in detail, by first evaluating the thermodynamically favorable oxygen insertion energies with GCMC in the simulation cell to identify regions of accessible volume within the polymer system. By subjecting each frame of an MD simulation to this treatment, it was possible to visualize the evolution of the energetically available space over time, with respect to oxygen and polymer movement. This atomistic insight is depicted in figure 13, whereby the evolution of accessible volume and

temporary channel formation can be seen over the course of an oxygen jump (a higher frame rate video of this is available in the supporting information). Through this analysis, it is noted that sites of accessible volume exist within the polymer framework; however, their location, volume, morphology and even existence varies significantly over time, due to the chain dynamics of the surrounding polymer network. The convergence of sites is observed to be sporadic; this appears to be temporary with channels frequently connecting and disconnecting over a longer time frame. Should an oxygen molecule be moving in the correct direction with sufficient velocity, it is able to traverse the length of the converged hole. This hopping motion is almost instantaneous, and is associated with a characteristic sudden increase in RMSD of 6-8 Å in under 4 ps.

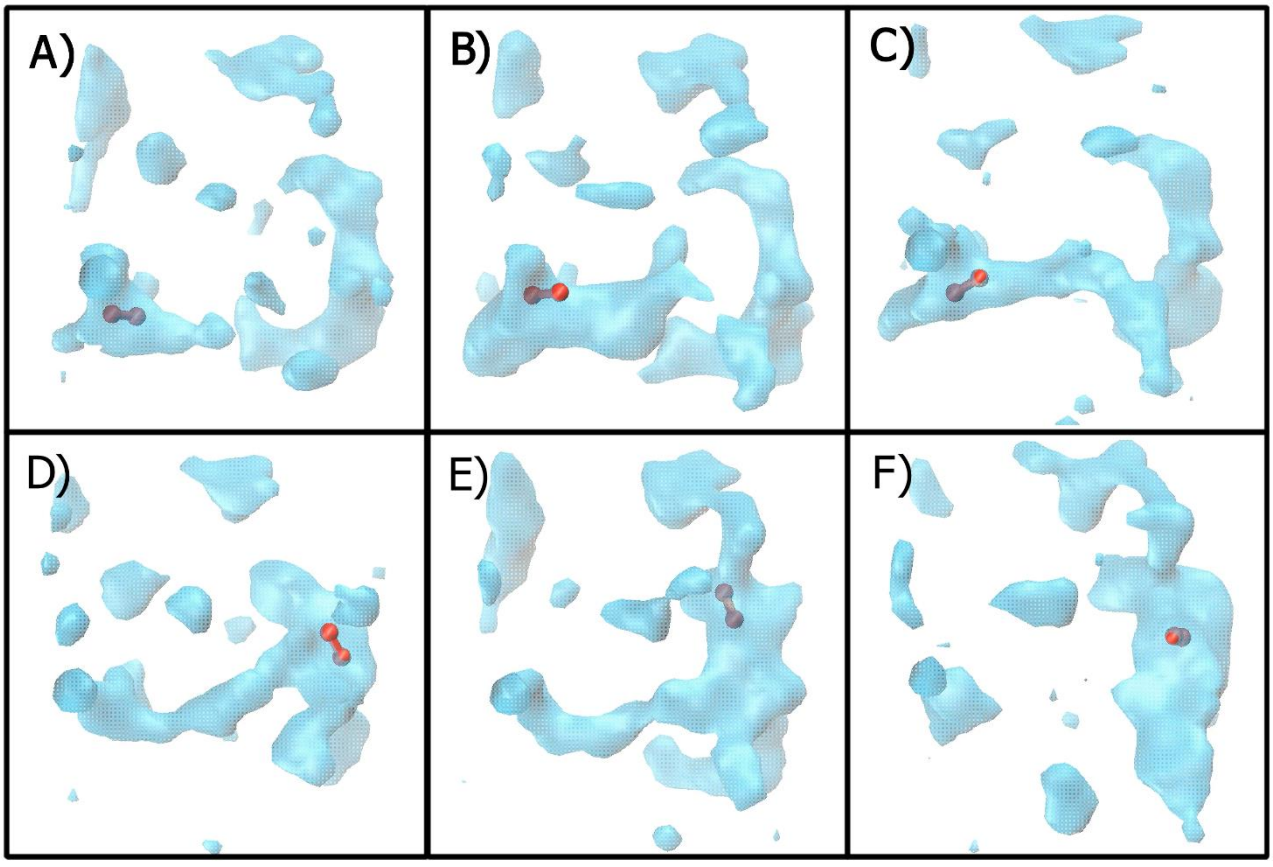

Figure 13. Images A) to F) show chronological snapshots of oxygen in a PEF system with respect to areas of free volume, demonstrating the hopping behavior over time. Trajectories have been

extracted from MD simulation. Frames have been subject to subsequent GCMC simulations to identify energetically available regions with respect to polymer and oxygen location within the system.

The importance of system density to this mechanism is therefore paramount as a more compact system will lead to fewer convergences between accessible volumes. It is likely that the increase in density between PEF and PET is predominantly responsible for the large decrease in diffusion coefficient,[67] with other factors such as interaction and chain dynamic energetics also contributing, albeit to a smaller extent.

CONCLUSION

In this study, all-atom models of both amorphous and crystalline PET and PEF were built and simulated using molecular dynamics. We demonstrated that the OPLS_2005 forcefield is reliable for these polymers, by comparing the simulations with both electronic structure calculations and experiment. These include the energetic values for binding and deformation, calculated via the OPLS forcefield and DFT, which compared favorably with one another. In addition, close attention was paid to the dihedral distributions of carbonyl to aromatic bonds, as such ring flipping motions are acknowledged to be important to the diffusion mechanism. Not only did these distributions match that observed experimentally through infrared studies, but the energy barrier for rotation was determined to be approximately a third higher in furan than in phenyl analogues (31.0 $kJ.mol^{-1}$ and 24.4 $kJ.mol^{-1}$ respectively). This resulted in fewer occurrences of ring flipping in realistic PEF systems, compared to PET, in agreement with existing experimental observations.[15]

We have also shown that reliable relative diffusion coefficients for oxygen transport through PEF and PET amorphous systems can be calculated. In order to have an improved description of amorphous polymers, for both sets of polymers, four systems of increasing degree of polymerization were simulated and, for each scale, five duplicate 200 ns simulations were considered in order to calculate oxygen diffusion coefficients. We found that the average oxygen diffusion coefficient was 11.3 times higher in PET compared to PEF, which shows good agreement with the experimental value of 11.2. There were differences in the absolute values of the average oxygen diffusion coefficient, where the calculated were 2.88×10^{-9} $cm^2.s^{-1}$ and 3.24×10^{-8} $cm^2.s^{-1}$, compared to experiment 1.04×10^{-9} $cm^2.s^{-1}$ and 1.16×10^{-8} $cm^2.s^{-1}$ for PEF and PET respectively. However, predicted transport coefficients by this method matched the accuracy of the more challenging TST method, and highlight the importance of simulation length and duplicate simulations on MSD calculations in dense polymer systems. Indeed, with continued future advances in computing resources and efficiency, it may be valuable to revisit these MD calculations and extend the simulations to the microsecond scale, to reduce the uncertainties still further. In considering both amorphous and crystalline systems separately, we have demonstrated that diffusion cannot proceed through the densely packed crystalline domains. In order to attain a more canonical representation of a synthetic semicrystalline system, future studies, requiring more demanding computing resources, could consider mixed systems of crystalline domains incorporated into an amorphous polymer matrix.

Another benefit of using these computational studies is that it was possible to gain new mechanistic insight into the diffusion of oxygen through PEF and PET. A closer analysis of the method of diffusion indicated that, whist a fourfold increase in ring-flipping activities increased the speed of penetrant diffusion by a factor of two, it could not solely account for the tenfold

discrepancy in oxygen diffusion between PET and PEF. Density and energetic interactions between penetrant and polymer were concluded to be of greater significance. The importance of system density in particular was highlighted when considering the method for which oxygen diffusion is achieved, with respect to the dynamics of the empty space which surrounds the polymer. Lateral penetrant diffusion may only occur when adjacent regions of empty space become connected. When one of these cages is occupied, oxygen has the opportunity to move typically 6-8 Å to traverse the newly converged site. It follows that decreased chain dynamics and a compact system leads to fewer connections between sites, therefore resulting in a smaller diffusion coefficient - as evidenced by oxygen diffusion in PEF systems relative to those of PET.

Thus, we consider that this simple and versatile approach successfully predicts barrier properties of plastics and, as demonstrated, is able to provide mechanistic insight into the diffusion pathway. Moreover, the general approach proposed here indicates a wider applicability to model gas transport in other polymer systems.

SUPPORTING INFOMATION

Modified dihedral terms of OPLS_2005 force field in modelling PEF; Oxygen mean squared displacement plots; Logarithmic oxygen mean squared displacement plots; Collective oxygen trajectories over 200 ns in PEF. (PDF).

Visualization of an oxygen jump with respect to energetically favorable areas of free volume throughout the polymer matrix (MOV).

AKNOWLEDGMENT

This research made use of the Balena High Performance Computing (HPC) Service at the University of Bath and the ARCHER UK National Supercomputing Service via our membership of the UK HEC Materials Chemistry Consortium (MCC; EPSRC EP/L000202, EP/R029431,

EP/T022213). The authors thank the UK EPSRC (EP/L016354/1, studentship to J. C. L., CDT in Sustainable Chemical Technologies), as well as the Royal Society (UF/160021 fellowship to A.B) for research funding.

REFERENCES

(1) Siracusa, V.; Blanco, I. Bio-Polyethylene (Bio-PE), Bio-Polypropylene (Bio-PP) and Bio-Poly(ethylene terephthalate) (Bio-PET): Recent Developments in Bio-Based Polymers Analogous to Petroleum-Derived Ones for Packaging and Engineering Applications. *Polymers* **2020**, *12*, 1641.

(2) Gopalakrishnan, P.; Narayan-Sarathy, S.; Ghosh, T.; Mahajan, K.; Belgacem, M. N. Synthesis and characterization of bio-based furanic polyesters. *Journal of Polymer Research* **2013**, *21*, 340.

(3) Romero-Hernández, O.; Romero Hernández, S.; Munõz, D.; Detta-Silveira, E.; Palacios-Brun, A.; Laguna, A. Environmental implications and market analysis of soft drink packaging systems in Mexico. A waste management approach. *The International Journal of Life Cycle Assessment* **2009**, *14*, 107–113.

(4) Groeninckx, G.; Reynaers, H.; Berghmans, H.; Smets, G. Morphology and melting behavior of semicrystalline poly(ethylene terephthalate): I. Isothermally crystallized PET. *J. Polym. Sci., Part B: Polym. Phys.* **1980**, *18*, 1311–1324.

(5) Liu, R. Y.; Hu, Y. S.; Schiraldi, D. A.; Hiltner, A.; Baer, E. Crystallinity and oxygen transport properties of PET bottle walls. *J Appl Polym Sci* **2004**, *94*, 671–677.

(6) Lin, J.; Shenogin, S.; Nazarenko, S. Oxygen solubility and specific volume of rigid amorphous fraction in semicrystalline poly(ethylene terephthalate). *Polymer* **2002**, *43*, 4733–4743.

(7) Rabnawaz, M.; Wyman, I.; Auras, R.; Cheng, S. A roadmap towards green packaging: the current status and future outlook for polyesters in the packaging industry. *Green Chem.* **2017**, *19*, 4737–4753.

(8) Loos, K.; Zhang, R.; Pereira, I.; Agostinho, B.; Hu, H.; Maniar, D.; Sbirrazzuoli, N.; Silvestre, A. J. D.; Guigo, N.; Sousa, A. F. A Perspective on PEF Synthesis, Properties, and End-Life. *Frontiers in Chemistry* **2020**, *8*, 585.

(9) Delidovich, I.; Hausoul, P. J. C.; Deng, L.; Pfützenreuter, R.; Rose, M.; Palkovits, R. Alternative Monomers Based on Lignocellulose and Their Use for Polymer Production. *Chem. Rev.* **2016**, *116*, 1540–1599.

(10) Eerhart, A. J. J. E.; Faaij, A. P. C.; Patel, M. K. Replacing fossil based PET with biobased PEF; process analysis, energy and GHG balance. *Energy & Environmental Science* **2012**, *5*, 6407–6422.

(11) Schultheis, M. W.; Shi, Y.; Moffitt, R. D.; You, X.; Kriegel, R. M. Furanoic Polymer Preforms, Containers and Processing. Patent WO2015031907A1, 5 March, 2015.

(12) Zimmer, J.; Dabrowski, N.; Teniere, V. Bottle, Method of Making the Same and Use of FDCA and Diol Monomers in Such Bottle. Patent WO2019115535A1, 20 June, 2019.

(13) Besson, J. P.; Bouffand, M. B.; Reutenauer, P. PEF container, preform & method for the manufacture of said container by injection stretch blow-molding. Patent WO2015015243, 5 February, 2015.

(14) Burgess, S. K. Fundamentals of Transport in Poly(ethylene terephthalate) and Poly(ethylene furanoate) Barrier Materials. Doctor of Philosophy Thesis, Georgia Institute of Technology, 2015.

(15) Burgess, S.; Leisen, J. E.; Kraftschik, B. E.; Mubarak, C. R.; Kriegel, R. M.; Koros, W. J. Chain Mobility, Thermal, and Mechanical Properties of Poly(ethylenefuranoate) Compared to Poly(ethylene terephthalate). *Macromolecules* **2014**, *47*, 1383–1391.

(16) Burgess, S. K.; Karvan, O.; Johnson, J. R.; Kriegel, R. M.; Koros, W. J. Oxygen sorption and transport in amorphous poly(ethylene furanoate). *Polymer* **2014**, *55*, 4748–4756.

(17) Wang, J.; Gardner, D. J.; Stark, N. M.; Bousfield, D. W.; Tajvidi, M.; Cai, Z. Moisture and Oxygen Barrier Properties of Cellulose Nanomaterial-Based Films. *ACS Sustainable Chem. Eng.* **2018**, *6*, 49–70.

(18) Burgess, S. K.; Wenz, G. B.; Kriegel, R. M.; Koros, W. J. Penetrant transport in semicrystalline poly(ethylene furanoate). *Polymer* **2016**, *98*, 305–310.

(19) Burgess, S. K.; Kriegel, R. M.; Koros, W. J. Carbon Dioxide Sorption and Transport in Amorphous Poly(ethylene furanoate). *Macromolecules* **2015**, *48*, 2184–2193.

(20) Burgess, S. K.; Mikkilineni, D. S.; Yu, D. B.; Kim, D. J.; Mubarak, C. R.; Kriegel, R. M.; Koros, W. J. Water sorption in poly(ethylene furanoate) compared to poly(ethylene terephthalate). Part 2: Kinetic sorption. *Polymer* **2014**, *55*, 6870–6882.

(21) Araujo, C. F.; Nolasco, M. M.; Ribeiro-Claro, P. J. A.; Rudíc, S.; Silvestre, A. J. D.; Vaz, P. D.; Sousa, A. F. Inside PEF: Chain Conformation and Dynamics in Crystalline and Amorphous Domains. *Macromolecules* **2018**, *51*, 3515–3526.

(22) Zhang, D.; Dumont, M.-J. Advances in polymer precursors and bio-based polymers synthesized from 5-hydroxymethylfurfural. *J. Polym. Sci., Part A: Polym. Chem.* **2017**, *55*, 1478–1492.

(23) Sun, L.; Wang, J.; Mahmud, S.; Jiang, Y.; Zhu, J.; Liu, X. New insight into the mechanism for the excellent gas properties of poly(ethylene 2,5-furandicarboxylate) (PEF): Role of furan ring's polarity. *Eur. Polym. J.* **2019**, *118*, 642–650.

(24) Gusev, A. A.; Arizzi, S.; Suter, U. W.; Moll, D. J. Dynamics of light gases in rigid matrices of dense polymers. *J. Chem. Phys.* **1993**, *99*, 2221–2227.

(25) Gusev, A. A.; Müller-Plathe, F.; Van Gunsteren, W. F.; Suter, U. W. Dynamics of small molecules in bulk polymers. In *Atomistic Modeling of Physical Properties*; Monnerie, L., Suter, U. W., Eds.; Springer Berlin Heidelberg: Berlin, Heidelberg, 1994; Chapter pp 207–247.

(26) Gusev, A. A.; Suter, U. W. Dynamics of small molecules in dense polymers subject to thermal motion. *J. Chem. Phys.* **1993**, *99*, 2228–2234.

(27) Ullal, V.; Spearot, D. E. Molecular dynamics simulation of O_2 diffusion in polydimethylsiloxane (PDMS) and end-linked PDMS networks. *Mol. Simul.* **2014**, *40*, 976– 986.

(28) Pant, P. V. K.; Boyd, R. H. Simulation of diffusion of small-molecule penetrants in polymers. *Macromolecules* **1992**, *25*, 494–495.

(29) Müller-Plathe, F. Molecular dynamics simulation of gas transport in amorphous polypropylene. *J. Chem. Phys.* **1992**, *96*, 3200–3205.

(30) Mueller-Plathe, F.; Rogers, S. C.; Van Gunsteren, W. F. Diffusion coefficients of penetrant gases in polyisobutylene can be calculated correctly by molecular-dynamics simulations. *Macromolecules* **1992**, *25*, 6722–6724.

(31) Müller-Plathe, F.; Rogers, S. C.; van Gunsteren, W. F. Gas sorption and transport in polyisobutylene: Equilibrium and nonequilibrium molecular dynamics simulations. *J. Chem. Phys.* **1993**, *98*, 9895–9904.

(32) Shanks, R.; Pavel, D. Simulation of diffusion of O_2 and CO_2 in amorphous poly(ethylene terephthalate) and related alkylene and isomeric polyesters. *Mol. Simul.* **2002**, *28*, 939–969.

(33) Li, T.; Kildsig, D. O.; Park, K. Computer simulation of molecular diffusion in amorphous polymers. *J. Controlled Release* **1997**, *48*, 57–66.

(34) Pavel, D.; Shanks, R. Molecular dynamics simulation of diffusion of O_2 and CO_2 in amorphous poly(ethylene terephthalate) and related aromatic polyesters. *Polymer* **2003**, *44*, 6713–6724.

(35) Gray-Weale, A. A.; Henchman, R. H.; Gilbert, R. G.; Greenfield, M. L.; Theodorou, D. N. Transition-State Theory Model for the Diffusion Coefficients of Small Penetrants in Glassy Polymers. *Macromolecules* **1997**, *30*, 7296–7306.

(36) Karayiannis, N. C.; Mavrantzas, V. G.; Theodorou, D. N. Detailed Atomistic Simulation of the Segmental Dynamics and Barrier Properties of Amorphous Poly(ethylene terephthalate) and Poly(ethylene isophthalate). *Macromolecules* **2004**, *37*, 2978–2995.

(37) *Gsnet & Gsdif Macros*; Accelrys Inc.: San Diego, CA, 1999.

(38) Fu, C.-F.; Tian, S. X. A Comparative Study for Molecular Dynamics Simulations of Liquid Benzene. *J. Chem Theory Comput.* **2011**, *7*, 2240–2252.

(39) Damm, W.; Frontera, A.; Tirado–Rives, J.; Jorgensen, W. L. OPLS all-atom force field for carbohydrates. *J. Comput. Chem.* **1997**, *18*, 1955–1970.

(40) Yong, C. W. Descriptions and Implementations of DL_F Notation: A Natural Chemical Expression System of Atom Types for Molecular Simulations. *J. Chem. Inf. Model* **2016**, *56*, 1405–1409

(41) Javanainen, M.; Vattulainen, I.; Monticelli, L. On Atomistic Models for Molecular Oxygen. *J. Phys. Chem. B* **2017**, *121*, 518–528.

(42) Mao, Y.; Kriegel, R. M.; Bucknall, D. G. The crystal structure of poly(ethylene furanoate). *Polymer* **2016**, *102*, 308–314.

(43) Chen, L. Polyethylene Terephthalate (Perfect crystal) 3856. 2018; https://khazana.

gatech.edu/module_search/material_detail.php?id=3858&m=9.

(44) Watson, G. W.; Kelsey, E. T.; de Leeuw, N. H.; Harris, D. J.; Parker, S. C. Atomistic simulation of dislocations, surfaces and interfaces in MgO. *J. Chem. Soc., Faraday Trans.* **1996**, *92*, 433–438.

(45) Todorov, I. T.; Smith, W.; Trachenko, K.; Dove, M. T. DL POLY 3: new dimensions in molecular dynamics simulations via massive parallelism. *J. Mater. Chem.* **2006**, *16*, 1911–1918.

(46) Frisch, M. J. et al. Gaussian 16, Revision A.03. 2016.

(47) Hafner, J.; Kresse, G. The Vienna AB-Initio Simulation Program VASP: An Efficient and Versatile Tool for Studying the Structural, Dynamic, and Electronic Properties of Materials. In *Properties of Complex Inorganic Solids*; Gonis, A., Meike, A., Turchi, P. E. A., Eds.; Springer US: Boston, MA, 1997; pp 69–82.

(48) Kresse, G.; Hafner, J. Ab initio molecular-dynamics simulation of the liquid-metal–amorphous-semiconductor transition in germanium. *Phys. Rev. B: Condens. Matter Mater. Phys.* **1994**, *49*, 14251– 14269.

(49) Kresse, G.; Furthmu¨ller, J. Efficient iterative schemes for ab initio total-energy calculations using a plane-wave basis set. *Phys. Rev. B: Condens. Matter Mater. Phys.* **1996**, *54*, 11169–11186.

(50) Zhu, R.; Molinari, M.; Shapley, T. V.; Parker, S. C. Modeling the Interaction of Nanoparticles with Mineral Surfaces: Adsorbed C60 on Pyrophyllite. *J. Phys. Chem. A* **2013**, *117*, 6602–6611.

(51) Kliměs, J.; Bowler, D. R.; Michaelides, A. Van der Waals density functionals applied to solids. *Phys. Rev. B: Condens. Matter Mater. Phys.* **2011**, *83*, 195131.

(52) Purton, J. A.; Crabtree, J. C.; Parker, S. C. DL MONTE: a general purpose program for parallel Monte Carlo simulation. *Mol. Simul.* **2013**, *39*, 1240–1252.

(53) Lindahl,; Abraham,; Hess,; van der Spoel, GROMACS 2019.2 Source code. 2019; https: //doi.org/10.5281/zenodo.2636382.

(54) Pronk, S.; Páll, S.; Schulz, R.; Larsson, P.; Bjelkmar, P.; Apostolov, R.; Shirts, M. R.; Smith, J. C.; Kasson, P. M.; van der Spoel, D.; Hess, B.; Lindahl, E. GROMACS 4.5: a high-

throughput and highly parallel open source molecular simulation toolkit. *Bioinformatics* **2013**, *29*, 845–854.

(55) Berendsen, H. J. C.; van der Spoel, D.; van Drunen, R. GROMACS: A message-passing parallel molecular dynamics implementation. *Comput. Phys. Commun.* **1995**, *91*, 43–56.

(56) Liu, J.; Geil, P. H. Crystal structure and morphology of poly(ethylene terephthalate) single crystals prepared by melt polymerization. *J. Macromol. Sci., Part B: Phys.* **1997**, *36*, 61–85.

(57) Berg, A.; Peter, C.; Johnston, K. Evaluation and Optimization of Interface Force Fields for Water on Gold Surfaces. *J. Chem. Theory Comput.* **2017**, *13*, 5610–5623.

(58) Huang, H. S.; Ai, L. Q.; van Duin, A. C. T.; Chen, M.; Lü, Y. J. ReaxFF reactive force field for molecular dynamics simulations of liquid Cu and Zr metals. *J. Chem. Phys.* **2019**, *151*, 94503.

(59) Dasetty, S.; Meza-Morales, P. J.; Getman, R. B.; Sarupria, S. Simulations of interfacial processes: recent advances in force field development. *Curr. Opin. Chem. Eng.* **2019**, *23*, 138–145.

(60) Fiorentini, V.; Methfessel, M. Extracting convergent surface energies from slab calculations. *J. Phys.: Condens. Matter* **1996**, *8*, 6525.

(61) Tran, R.; Xu, Z.; Radhakrishnan, B.; Winston, D.; Sun, W.; Persson, K. A.; Ong, S. P. Surface energies of elemental crystals. *Scientific Data* **2016**, *3*, 160080.

(62) Parker, S. C.; Kerisit, S.; Marmier, A.; Grigoleit, S.; Watson, G. W. Modelling inorganic solids and their interfaces: A combined approach of atomistic and electronic structure simulation techniques. *Faraday Discuss.* **2003**, *124*, 155–170.

(63) Codou, A.; Moncel, M.; van Berkel, J. G.; Guigo, N.; Sbirrazzuoli, N. Glass transition dynamics and cooperativity length of poly(ethylene 2,5-furandicarboxylate) compared to poly(ethylene terephthalate). *Phys. Chem. Chem. Phys.* **2016**, *18*, 16647–16658.

(64) Karimi, M. Diffusion in Polymer Solids and Solutions. In *Mass Transfer in Chemical Engineering Processes*; Markŏs, J., Ed.; Books on Demand, 2011; pp 17–40.

(65) Trifol, J.; Plackett, D.; Szabo, P.; Daugaard, A. E.; Giacinti Baschetti, M. Effect of Crystallinity on Water Vapor Sorption, Diffusion, and Permeation of PLA-Based Nanocomposites. *ACS Omega* **2020**, *5*, 15362–15369.

(66) Takeuchi, H. A jump motion of small molecules in glassy polymers: A molecular dynamics simulation. *J. Chem. Phys.* **1990**, *93*, 2062–2067.

(67) Cozmuta, I.; Blanco, M.; Goddard, W. A. Gas Sorption and Barrier Properties of Polymeric Membranes from Molecular Dynamics and Monte Carlo Simulations. *J. Phys. Chem. B* **2007**, *111*, 3151–3166.